Progress In Electromagnetics Research, Vol. 136, 385–407, 2013

SAR TARGET CLASSIFICATION USING BAYESIAN COMPRESSIVE SENSING WITH SCATTERING CENTERS FEATURES

Xinzheng Zhang[1, *], Jianhong Qin[1], and Guojun Li[2]

[1]College of Communication Engineering, Chongqing University, Chongqing 400044, China

[2]Department of Communication Commanding, Chongqing Communication Institute, Chongqing 400035, China

Abstract—The emerging field of compressed sensing provides sparse reconstruction, which has demonstrated promising results in the areas of signal processing and pattern recognition. In this paper, a new approach for synthetic aperture radar (SAR) target classification is proposed based on Bayesian compressive sensing (BCS) with scattering centers features. Scattering centers features is extracted as a l_1-norm sparse problem on the basis of SAR observation physical model, which can improve discrimination ability compared with original SAR image. Using an overcomplete dictionary constructed by training samples, BCS is utilized to design targets classifier. For target classification performance evaluation, the proposed method is compared with several state-of-art methods through experiments on Moving and Stationary Target Acquisition and Recognition (MSTAR) public release database. Experiment results illustrate the effectiveness and robustness of the proposed approach.

1. INTRODUCTION

Synthetic aperture radar (SAR) is a microwave sensor which has the ability to produce all-weather, 24-hour a day, high-resolution images [1, 2]. A SAR system sends electromagnetic pulses from a radar mounted on an airborne or spaceborne platform to a particular area of interest on the ground and records the return signals. In order to achieve high cross-range resolution, SAR collects data from multiple observation points, and focuses the received information coherently

Received 7 December 2012, Accepted 11 January 2013, Scheduled 20 January 2013

* Corresponding author: Xinzheng Zhang (zhangxinzheng03@126.com).

to obtain a high-resolution description of the scene. Automatic Target Recognition (ATR) systems using SAR sensors continue to be developed for a wide variety of applications, particularly in the area of military defense [3, 4]. The goal of these ATR systems is to detect and classify military targets using various image and signal processing techniques. The conventional multistage ATR algorithm consists of three separate stages: The pre-screener identifies local regions of interest using a Constant False Alarm Rate (CFAR) detector, allowing all targets and numerous false alarms to pass. It is followed by a one-class discriminator which aims to eliminate all natural false alarms, also referred to as clutter. Finally, the classifier receives all man-made objects and attempts to categorize each input image as a specific target type contained in the training set or to reject the object as man-made clutter. General reviews of automatic target recognition concepts and the SAR targets detection technologies can be found in [5].

The performance of a SAR ATR system is mainly decided by features extraction and classification algorithms [6]. A number of different feature extraction methods exist for the exploitation of SAR target images with respect to target classification. One popular approach towards target classification is to use a SAR target image's amplitude values to directly generate image features. These image features can be used with common classifiers like nearest neighbor or neural networks. In addition to target image, the shadows in SAR image is also used as features for SAR ATR [7]. Principle component analysis (PCA) and independent component analysis (ICA) are popular features extraction approaches for target classification [6, 8, 9]. SAR data, however, does not necessarily need to be processed as a single image. A single SAR image can be filtered to form multiple sub-aperture images, and features can be extracted from each sub-image [10]. A further breakdown of SAR data is the use of high resolution range (HRR) profiles as one-dimensional target features. The HRR profiles can be processed to extract one-dimensional scattering centers or time-frequency features [11, 12]. A SAR target image can be well approximated as a sum of two-dimensional scattering centers which provide a concise, yet physically relevant description of the target [13–15]. But the conventional parametric scattering centers feature extraction is very complicate and very hard to solve. In this paper, we propose a new scattering centers feature extraction technique based on sparse nature of scattering centers. In this technique, scattering centers features are extracted as a l_1-norm sparse problem.

As for classification algorithms, the template matching is commonly used in which multiple templates for each target are

generated at incrementally spaced aspect angles. The addition of a target to the training set requires only the creation of an additional set of templates. However, these schemes become computationally intensive as the number of templates and target types are increased. The other popular classification approach uses the support vector machine (SVM) which are typically nonlinear [16]. SVM based approaches have been shown to outperform conventional template-based approaches, providing better generalization capabilities. For classification tasks, SVM has advantages of elegant mathematical tractability and working with a relatively small number of training samples [17–20]. But SVM cannot allow the number of supports to be adapted to the specific signal being characterized. These pattern recognition approaches utilize a set of classifiers, each developed using target training images over a given range of aspect angles. While these classification systems achieve reduced complexity, the approaches are reliant on an accurate target pose angle estimate.

In this paper, we design SAR target classifier utilizing compressive sensing (CS) theory without target pose estimation. The recently-emerged CS theory, which originally aims to address signal reconstruction and coding problems, has shown tremendous potential for pattern recognition application [21–23]. CS has shown success in face recognition over linear SVM and 1-nearest neighbor (1-NN) methods [24–26]. Differently from techniques such as linear discriminant analysis (LDA) and SVM, CS is not learned from a training set and therefore does not suffer from limited generalization. In [27], sparse representation is employed to develop SAR ATR method. However, SAR target images is used as features directly in the work, in which ATR performance are affected by ground clutter. Recent works have attempted to incorporate CS reconstruction in a Bayesian framework which is called Bayesian compressive sensing (BCS) [28]. BCS accounts for noise and has a much better performance in noisy condition. Motivated by those above, a new approach of SAR target classification is presented based on the BCS theory with scattering centers features and without target pose estimation. In our approach, on one hand, scattering centers are used as features instead of original SAR target image, which can reduce clutter effect for ATR. On the other hand, BCS is used to design classifier, which can improve ATR performance in noise condition.

The rest of this paper is organized as follows: in Section 2, scattering centers features extraction with sparse constraint is investigated. In Section 3, the theoretical background of Bayesian compressive sensing (BCS) is reviewed briefly, and how BCS is applied as a classifier is described. The experiment verification using Moving

and Stationary Target Acquisition and Recognition (MSTAR) public release database is presented in detail in Section 4. Finally, the conclusions are summarized in Section 5.

2. SCATTERING CENTERS FEATURES EXTRACTION WITH SPARSE CONSTRAINT

SAR imaging is an inverse scattering problem whereby a spatial map of reflectivity is reconstructed from measurements of scattered electric fields. Imaging techniques to exploit parsimony in sparse or compressible scenes have been proposed throughout the development of radar processing for superresolution of scattering locations and features extraction [29]. For a SAR target image, the scattering response of a target can be well approximated as a sum of responses from sparse individual reflectors. Since SAR target classification tasks usually rely on features of dominant point scattering centers [29, 30], we extract point scattering centers from the view of sparsity exploitation.

The physical model for the SAR observation process can be formulated as following [31]:

$$\mathbf{r} = \mathbf{C}\mathbf{u} + \mathbf{w} \tag{1}$$

where $\mathbf{r}$ are the SAR observations data. $\mathbf{u}$ is the unknown sampled reflectivity image, $\mathbf{w}$ the additive measurement noise, and $\mathbf{C}$ a SAR observation matrix. Here, phase history data converted from a complex SAR image are used, so a 2D Fourier-type operator is adopted for $\mathbf{C}$. The procedure converting a complex SAR image to phase history data is detailed in [11]. In this framework, the objective of SAR target point scattering centers features extraction is to obtain a sparse estimate of $\mathbf{u}$ based on the data $\mathbf{r}$. So, we formulate the problem as an optimization problem of the following form:

$$\hat{\mathbf{u}} = \arg\min_{\mathbf{u}} \left[\|\mathbf{r} - \mathbf{C}\mathbf{u}\|_2^2 + \lambda \|\mathbf{u}\|_0 \right] \tag{2}$$

where $\|\cdot\|_2$ denotes the l_2-norm, $\|\cdot\|_0$ the l_0-norm, and λ the l_0-norm regularization parameter. The first term in the above objective function is a data fidelity term. The second term reflect the prior information concerning the sparse behavior of $\mathbf{u}$ that we would like to impose. Use of l_0-norm constraints, such as those in Equation (2), has become a sparse features extraction due to the ability of these constraints to prevent suppression of useful features in the image. Due to l_0-norm, exact determination of sparsest representation Equation (2) proves to be an NP-hard problem [22, 23]. Thus, approximate solutions are considered instead by replacing the l_0-norm with l_1-norm [23]. So,

Equation (2) can be rewritten as follows:

$$\hat{\mathbf{u}} = \arg\min_{\mathbf{u}} \left[\|\mathbf{r} - \mathbf{C}\mathbf{u}\|_2^2 + \lambda \|\mathbf{u}\|_1 \right] \tag{3}$$

In order to avoid problems due to non-differentiability of the l_1-norm [31], a smooth approximation to the l_1-norm is used in (3):

$$\|\mathbf{u}\|_1 \approx \sum_{i=1}^{K} \left(|(\mathbf{u})_i|^2 + \varsigma \right)^{1/2} \tag{4}$$

where $\varsigma \geq 0$ is a small constant, K the length of the complex vector $\mathbf{u}$, and $(\mathbf{u})_i$ the ith element of $\mathbf{u}$. So Equation (3) can be rewritten using the modified cost function as follows:

$$J(\mathbf{u}) = \arg\min_{\mathbf{u}} \left[\|\mathbf{r} - \mathbf{C}\mathbf{u}\|_2^2 + \lambda \sum_{i=1}^{K} \left(|(\mathbf{u})_i|^2 + \varsigma \right)^{1/2} \right] \tag{5}$$

To solve the problem of Equation (5), we adopt the quasi-Newton method in [31] which can account for the complex-valued nature of the SAR problem. The solution procedure is briefly described here. A structure is used which effectively deals with both the complex-valued nature of $\mathbf{u}$ and the nonlinearity associated with $|\mathbf{u}|$. The gradient of (5) is firstly taken with respect to the real and imaginary parts of $\mathbf{u}$. This yields a gradient vector of length $2K$. Then, this vector is put into a compact form, by defining a complex-valued gradient vector of length K, whose real and imaginary components contain the derivatives with respect to the real and imaginary parts of $\mathbf{u}$ respectively. This compact gradient can be placed in the following useful form following substantial manipulation:

$$\nabla J(\mathbf{u}) = \tilde{H}(\mathbf{u})\mathbf{u} - 2\mathbf{C}^H\mathbf{r} \tag{6}$$

where

$$\begin{aligned} \tilde{H}(\mathbf{u}) &\triangleq 2\mathbf{C}^H\mathbf{C} + k\lambda L(\mathbf{u}) \\ L(\mathbf{u}) &\triangleq \operatorname{diag}\left\{ \frac{1}{\left(|(\mathbf{u})_i|^2 + \varsigma \right)^{1/2}} \right\} \end{aligned} \tag{7}$$

where $(\cdot)^H$ denotes the Hermitian of a matrix, and $\operatorname{diag}\{\cdot\}$ is a diagonal matrix whose ith diagonal element is given by the expression inside the brackets. The term $\tilde{H}(\mathbf{u})$ is used as an approximation to the Hessian and used in the following quasi-Newton iteration:

$$\hat{\mathbf{u}}^{(n+1)} = \hat{\mathbf{u}}^{(n)} - \gamma \left[\tilde{H}\left(\hat{\mathbf{u}}^{(n)} \right) \right]^{-1} \nabla J\left(\hat{\mathbf{u}}^{(n)} \right) \tag{8}$$

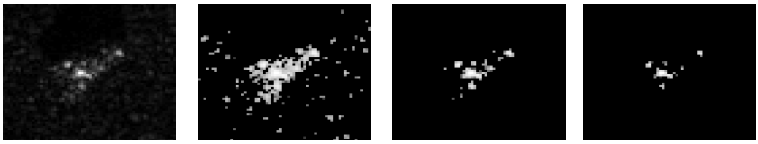

(a) (b) (c) (d)

Figure 1. (a) SAR target image. (b) Scattering centers with $\lambda = 1$. (c) Scattering centers with $\lambda = 4$. (d) Scattering centers with $\lambda = 9$.

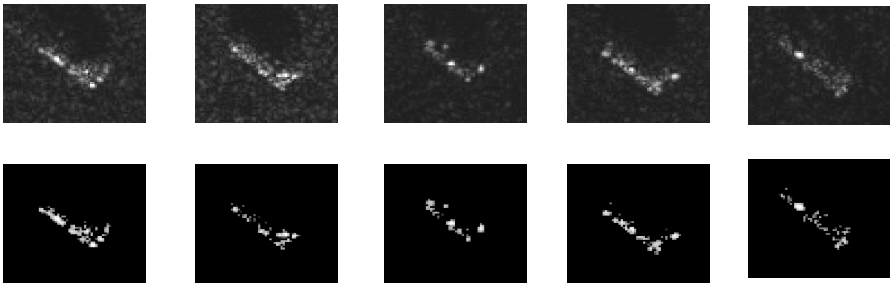

(a) (b) (c) (d) (e)

Figure 2. The first row is SAR image chips of different targets, the second row is the corresponding scattering centers. (a) BMP2 target. (b) BTR70 target. (c) BRDM2 target. (d) T72 target. (e) ZIL131 target.

where γ is the step size. Subsituting (6) into (8), the iterative algorithm can be obtained:

$$\tilde{H}\left(\hat{\mathbf{u}}^{(n)}\right) \cdot \hat{\mathbf{u}}^{(n+1)} = (1-\gamma)\tilde{H}\left(\hat{\mathbf{u}}^{(n)}\right)\hat{\mathbf{u}}^{(n)} + 2\gamma \mathbf{C}^H \mathbf{r} \tag{9}$$

The iteration (9) is runned until $\|\hat{\mathbf{u}}^{(n+1)} - \hat{\mathbf{u}}^{(n)}\|_2^2 / \|\hat{\mathbf{u}}^{(n)}\|_2^2 < \upsilon$, where $\upsilon > 0$ is a small constant.

The value of λ can be determined through experiments. We show some experiments results in the following figures. Figure 1 depicts sparse scattering centers of the same SAR target image with different λ. From Figure 1, it can be seen that the value of λ effects sparsity of extracted features, a relatively large λ may lose some low-amplitude scattering centers, but a relatively small λ may reserve a little clutter or artifacts. Through experiments, we find that $\lambda = 4$ is appropriate. Figure 2 show some sparse scattering centres examples with different SAR targets image chips in MSTAR public release database. From these results, it can be found that dominant scattering centers are extracted with all ground clutter removed.

3. SAR TARGET CLASSIFICATION USING COMPRESSIVE SENSING

3.1. General Theory of Compressive Sensing

The general theory behind CS can be summarized as follows: let us assume that we are given a discrete signal, $\mathbf{x}$, in R^N and a $N \times N$ matrix, Ψ, whose columns are a set of orthogonal basis vectors. This matrix is called a sparsifying matrix since, when multiplied by signal $\mathbf{x}$, it produces a representation $\theta = \Psi^T \mathbf{x}$ which is a version of $\mathbf{x}$ in the Ψ domain. For many naturally occurring signals such as images and audio and an appropriate choice of Ψ, vector θ offers a sparse representation in the sense that only K of its elements have values significantly different from zero; the other $N - K$ elements of θ are either zero or very close to zero. In such a case, $\mathbf{x}$ is said to be K-sparse. Typical choices for Ψ are the discrete cosine transform matrix and the wavelet basis matrix, both widely used in image compression applications.

In addition to Ψ, a linear measurement matrix or sampling matrix Φ of size $M \times N$ is also introduced, with $M \ll N$ and M only marginally larger than K such that:

$$\mathbf{y} = \Phi\mathbf{x} = \Phi\Psi\theta = \Theta\theta \tag{10}$$

Vector $\mathbf{y}$ contains the measurements in R^M which we can access directly. When Θ satisfies the so-called restricted isometry property (RIP), we can reconstruct θ given $\mathbf{y}$ exactly. The RIP, which is used to prove many theorems in the field of CS, characterizes matrices which are nearly orthonormal, at least when operating on sparse vectors [22, 23]. Details of the RIP is described in [22]. A thorough verification of RIP for Θ is prohibitive and requires computations in every $M \times K$ sub-matrix of Θ, which involves $\binom{N}{K}$ combinations [21–23]. Yet, it can be shown that if Φ is chosen to be a Gaussian random matrix and condition $M \geq cK\log(N/K)$ is satisfied for some constant c, then it is highly probable that we will be able to reconstruct θ exactly [21–23].

As described above, it is immediate that matrix Φ has more columns than rows equation in Equation (10). Therefore, θ lies in a solution space and cannot be reconstructed uniquely. However, thanks to the sparsity assumption, we can recover signal $\widehat{\theta}$ by minimizing its l_1 norm as follows:

$$\widehat{\theta} = \arg\min_{\theta} \left(\|\theta\|_1 \right), \quad s.t. \quad \mathbf{y} = \Theta\theta \tag{11}$$

Several other reconstruction algorithms have been presented in recent years including the basis pursuit (BP) algorithm and the least absolute shrinkage and selection operator (LASSO) algorithm [32, 33].

3.2. Compressive Sensing with Bayesian Framework

In the Bayesian compressive sensing formalism, rather than providing a point estimate of the signal, a full posterior density function is provided which can provide a much sparser signal than other CS reconstruction algorithms for noisy condition. In addition, the Bayesian framework takes into account of the additive noise encountered when implements compressed sampling [28].

In BCS, the Equation (3) is rewritten as following:

$$\mathbf{y} = \Theta\theta + \delta \tag{12}$$

where δ is a zero-mean Gaussian noise with uncertain variance σ^2. Then the Gaussian likelihood function of $\mathbf{y}$ is:

$$p\left(\mathbf{y}|\theta, \sigma^2\right) = \left(2\pi\sigma^2\right)^{-(M/2)} \exp\left\{-\left(1/2\sigma^2\right)\left\|\mathbf{y}-\Theta\theta\right\|^2\right\} \tag{13}$$

This above analysis has converted the CS problem of inverting for θ into a linear regression problem with a prior that θ is compressible. Assuming the knowledge of Θ, the quantities to be estimated based on the $\mathbf{Y}$ are the compressible weights θ and the noise variance σ^2.

In a Bayesian formalism, the fact that θ is compressible is formalised by placing a sparseness promoting prior on θ. A hierarchical prior is imposed on θ for carrying the Bayesian analysis further [28]. To see this, first define a zero-mean Gaussian prior on each element θ_i.

$$p(\theta|\alpha) = \prod_{i=1}^{K} N(\theta_i|0, \alpha_i^{-1}) \tag{14}$$

with α_i the precision of a Gaussian density function. Further, a Gamma prior is considered over α and the inverse of the noise variance $\alpha_0 = 1/\sigma^2$.

$$p(\alpha|a, b) = \prod_{i=1}^{M} \Gamma(\alpha_i|a, b) \tag{15}$$

$$p(\alpha_0|c, d) = \prod_{i=1}^{M} \Gamma(\alpha_i|c, d) \tag{16}$$

The relevant parameters are set to be zero such that $a = b = c = d = 0$ as that used in [28]. Then we can obtain the posterior distribution over θ is:

$$p(\theta|\alpha, \alpha_0) = N(\theta|\mu, \Sigma) \tag{17}$$

where the posterior mean and covariance are:

$$\mu = \alpha_0 \mathbf{\Sigma} \Theta^T \mathbf{y} \tag{18}$$

$$\Sigma = \left(\alpha_0 \Theta^T \Theta + \mathbf{A}\right) \tag{19}$$

with $\mathbf{A} = \text{diag}(\alpha_1, \alpha_2, \ldots, \alpha_M)$. By marginalising over the weights θ, the marginal likelihood for α and α_0 can be expressed as:

$$L(\alpha, \alpha_0) = -\frac{1}{2}\left(M \log 2\pi + \log |\mathbf{D}| + \mathbf{y}^T \mathbf{D}^{-1} \mathbf{y}\right) \tag{20}$$

with $\mathbf{D} = \sigma^2 \mathbf{I} + \Theta \mathbf{A}^{-1} \mathbf{A}^T$. A maximum likelihood (ML) approximation can be used to provide an estimation of α and α_0 as:

$$\alpha_i^{\text{new}} = \frac{s_i}{\mu_i}, \tag{21}$$

$$\alpha_0^{\text{new}} = \frac{M - \sum_{i=1}^{M} s_i}{\|\mathbf{s} - \Theta\mu\|_2^2} \tag{22}$$

where μ_i is the ith posterior mean weight form and $r_i = 1 - \alpha_i \Sigma_{ii}$.

Note that α_i^{new} and α_0^{new} are functions of μ and Σ, while μ and Σ are functions of α and α_0. This suggests an iterative algorithm, until a convergence criterion has been satisfied. The BCS formalism can not only provide a precise and sharp reconstruction of θ in noisy scene, but also it is much faster in contrast to other CS algorithms by using fast Relevant Vector Machine (RVM) algorithm [34, 35].

3.3. Classification Based on BCS

In this sub-section, we discuss how BCS can be used for SAR targets classification. The goal of classification is to use training data from k different classes to determine the best class to assign to test vector $\mathbf{z}$. First, let us consider taking all training examples n_i from class i and concatenate them into a matrix $\mathbf{B}_i$ as columns, other words $\mathbf{B}_i = [\mathbf{b}_{i,1}, \mathbf{b}_{i,2}, \ldots, \mathbf{b}_{i,n_i}] \in R^{M \times n_i}$, where $\mathbf{b} \in R^M$ represents a feature vector from the training set of class i with dimension m. Given sufficient training examples from class i, reference [25] shows that a test sample $\mathbf{z}$ from the same class can be represented as a linear combination of the entries in $\mathbf{B}_i$ weighted by β, that is:

$$\mathbf{z} = \beta_{i.,1}\mathbf{b}_{i.,1} + \beta_{i.,2}\mathbf{b}_{i.,2} + \ldots + \beta_{i.,n_i}\mathbf{b}_{i.,n_i} \tag{23}$$

However, since the class membership of $\mathbf{z}$ is unknown, we define a matrix $\mathbf{B}$ to include training examples from all k classes in the training set, in other words the columns of $\mathbf{B}$ are defined as $\mathbf{B} = [\mathbf{B}_1, \mathbf{B}_2, \ldots, \mathbf{B}_k] = [\mathbf{b}_{1,1}, \mathbf{b}_{1,2}, \ldots, \mathbf{b}_{k,n_k}] \in R^{M \times S}$. Here M is the

dimension of each vector $\mathbf{b}$ and N the total number of all training examples from all classes. We can then write test vector $\mathbf{z}$ as a linear combination of all training examples, in other words $\mathbf{z} = \mathbf{B}\beta$. Ideally the optimal β should be sparse, and only be non-zero for the elements in $\mathbf{B}$ will belong to the same class as $\mathbf{z}$. This motivates us to solve for the sparse representation of β using the BCS formulas presented in Section 3.

Now that we have described our method to solve for β is via BCS, we now discuss how to assign $\mathbf{z}$ as belonging to a specific class. Ideally, all nonzero entries of β should correspond to the entries in $\mathbf{B}$ with the same class as $\mathbf{z}$. In this ideal case, $\mathbf{z}$ will assign itself to one training example from $\mathbf{B}$, and we can assign $\mathbf{z}$ to the class which has the largest support in β. However, due to noise and modeling error, β belonging to other classes could potentially be non-zero. Therefore, we compute the l_2-norm for all β entries within a specific class, and choose the class with the largest l_2-norm support.

More specifically, let us define a selector $\eta_i(\beta) \in R^S$ as a vector whose entries are non-zero except for entries in β corresponding to class i. We then compute the l_2-norm for β for class i as $\|\eta_i(\beta)\|_2$. The best class for $\mathbf{z}$ will be the class in β with the largest l_2-norm. Mathematically, the best class $i^*_{\mathbf{z}}$ is defined as:

$$i^*_{\mathbf{z}} = \max_i \|\eta_i(\beta)\|_2 \tag{24}$$

4. EXPERIMENT RESULTS

4.1. Database

In this section, we evaluate the classification performance of the proposed approach using the popular MSTAR public database, which is a standard dataset for evaluating SAR ATR algorithms, consisting X-band SAR images with 1 ft $\times$ 1 ft resolution for ten targets. These ten targets are several military vehicles and a few civilian vehicles, including BMP2 (tank), BRDM2 (truck), BTR60 (armored car), BTR70 (armored car), D7 (bulldozer), T62 (tank), T72 (tank), ZIL131 (truck), ZSU23/4 (cannon), 2S1 (cannon). These targets have very similar shape. Visible light images of these targets are depicted in Figure 3, and SAR images for ten class targets at near poses are depicted in Figure 4. The data typically consists of target SAR image chips. For each target, images were acquired at 17° and 15° depression angles over the full 360° aspect angles. The data in depression 17° are used for training and the other for testing. Table 1 lists the type and sample number of training and testing sets.

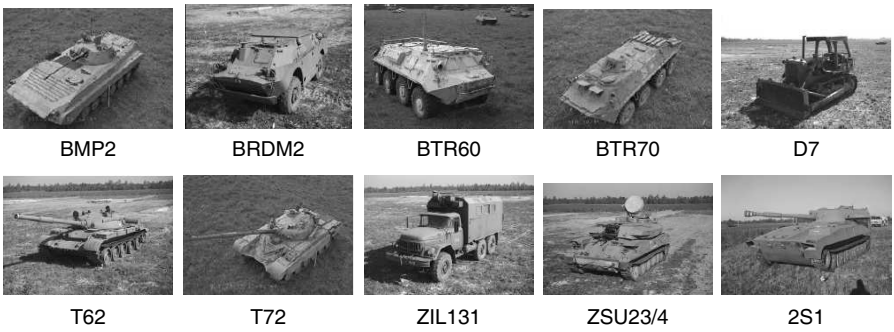

Figure 3. Visible light images for ten targets in MSTAR database.

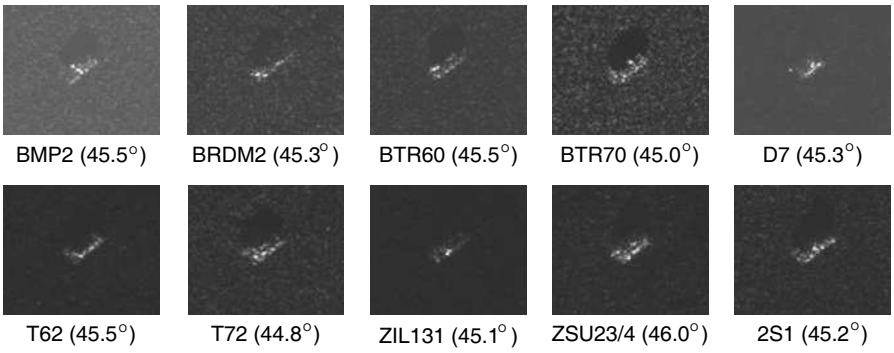

Figure 4. SAR images for ten targets at near aspect angles (the data in brackets is poses).

The main work before doing classification is the preprocessing. Because we want to classify the target (and not the clutter), it is not much meaningful to take the complete original images as input for the classifier. The preprocessing consists of several steps as following. Firstly, because of MSTAR target locating nearly in the center of chips, we can only extract a 64×64 sub-image in the center of a SAR original 128×128 image chip from the training and testing sets. Secondly, we normalize to one the l_2-norm of all the sub-images. Finally, scattering centers features are extracted after segmentation.

For comparison, we compare the proposed approach with several state-of-the-art methods: CS classifier based on BP, sparse representative classifier (SRC) and linear SVM with radial basis function (RBF) kernel. The principle of SRC is detailed in [25]. The LIBSVM package is used and one-against-all strategy for multi-class classification is adopted [27].

In the sequel, we will carry out several experiments. The performance of all methods is firstly evaluated on a 3-Class SAR target recognition problem with SAR image amplitude values and scattering centers features respectively. Then, the robustness of the proposed method is examined with respect to depression angle changes and noise. Finally, the proposed method is evaluated on the more challenging 10-class recognition problem.

4.2. 3-class Problem

In this experiment, we use the data from three classes (BMP2, BTR70 and T72) for algorithm evaluation and comparison. As shown in Table 1, there are 3 different serial numbers for BMP2 and T72. For these two targets, we only use the images from serial number SN_C21 for BMP2 and SN_132 for T72 at depression angle 17° as the training data. For testing, all images at depression angle 15° are used. The 3 target image set was chosen because there is available in the open literature a pilot study that can be used as a base for further comparisons.

Figure 5 shows an illustrative classification example using scattering centers features, in which the BCS sparse representation

Table 1. MSTAR datasets used in the recognition performance analysis.

No.	Type		Train (17°)	Test (15°)
1	BMP2	SN_C21	233	196
		SN_C9563	233	195
		SN_C9566	232	196
2	BRDM2		298	274
3	BTR60		256	195
4	BTR70		233	196
5	D7		299	274
6	T62		299	273
7	T72	SN_132	232	196
		SN_812	231	195
		SN_S7	228	191
8	ZIL131		299	274
9	ZSU234		299	274
10	2S1		299	274

coefficients are compared with BP and SRC respectively. In Figure 5, the sparse representation coefficients are shown by the stem plots, and the class-wise reconstruction errors are displayed by the bar plots. The same dictionary constructed with 3 target training samples is used in three compressive sensing methods. The test sample is from the class of BMP2 with pose of 27.8°. From Figure 5, it can be seen that all of the three compressive sensing methods can recognize the class label correctly for the test sample from the class of BMP2. However, Figure 5(f) shows that the reconstruction error from BCS

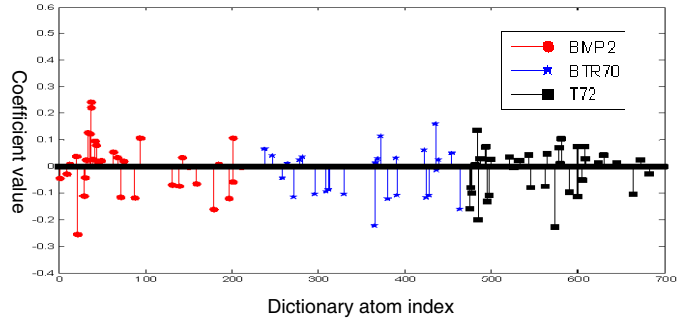

(a)

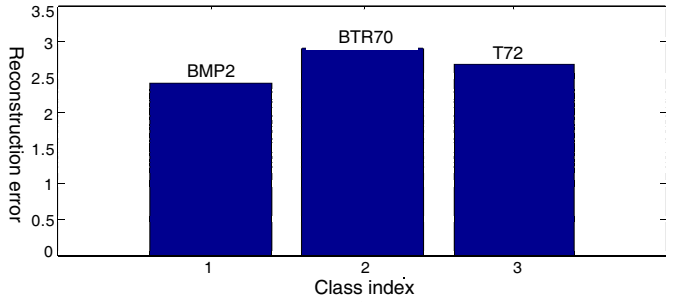

(b)

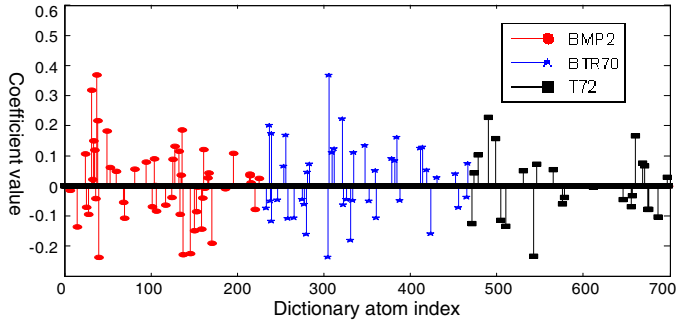

(c)

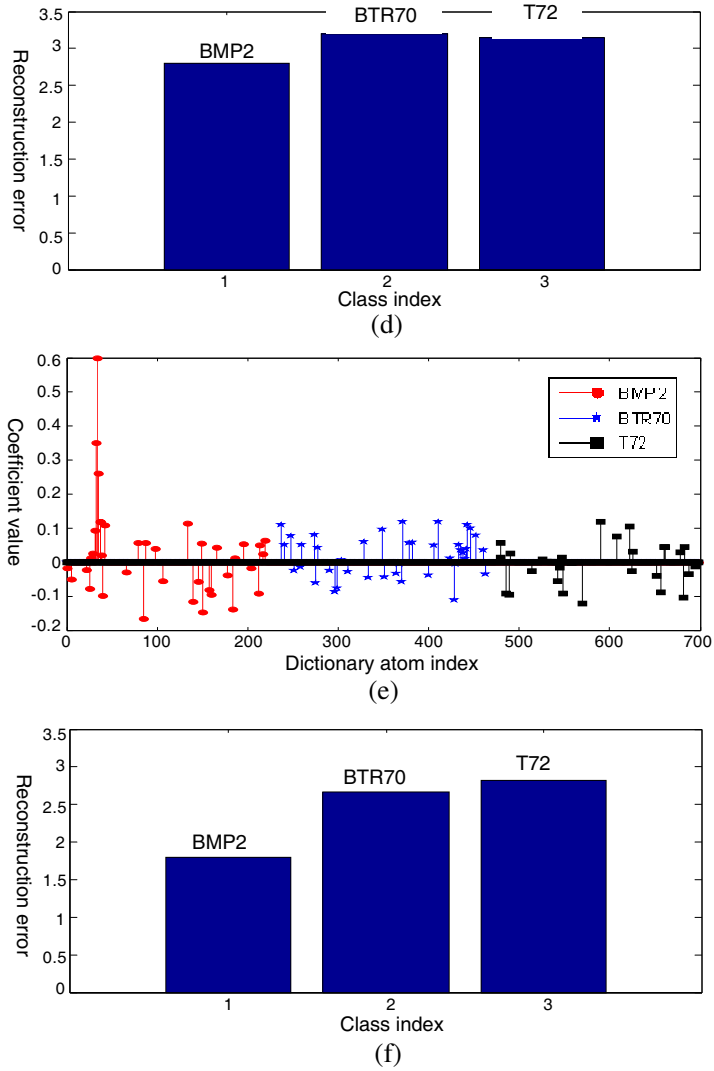

Figure 5. Examples of sparse coefficients and reconstruction errors using different classifiers on the 3-target datasets. BMP2 test sample classification via: (a) and (b) BP, (c) and (d) SRC, (e) and (f) BCS.

with scattering centers features is the smallest for the correct class, which indicates that BCS has a better confidence level on classification decision.

For another test sample from BMP2 with pose of 70.8°, Figure 6 shows the sparse coefficients and reconstruction errors by BCS

with scattering centers features and target image's amplitude values respectively. From Figure 6, it can be seen that features of amplitude values fails to classify the target while scattering centers features can classify the target correctly.

Table 2 displays the classification accuracy of four classifiers (BP, SRC, SVM and BCS) with scattering centers features. For comparison, Table 3 displays the classification accuracy of four classifiers with SAR

Table 2. Classification accuracy comparison of different classifiers with scattering centers features.

Features		Scattering centers			
Classifier		BP	SRC	SVM	BCS
Target	BMP2	87.2%	79.6%	77.1%	94.9%
	BTR70	93.4%	88.8%	87.2%	100%
	T72	92.7%	89.2%	87.5%	98.7%
ARA		91.1%	85.8%	83.9%	97.9%

Note: ARA means average recognition accuracy.

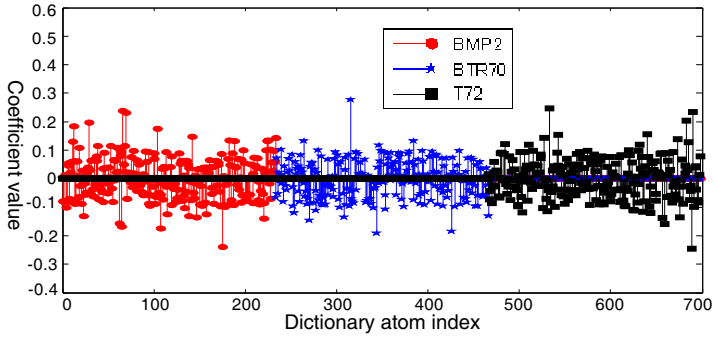

(a)

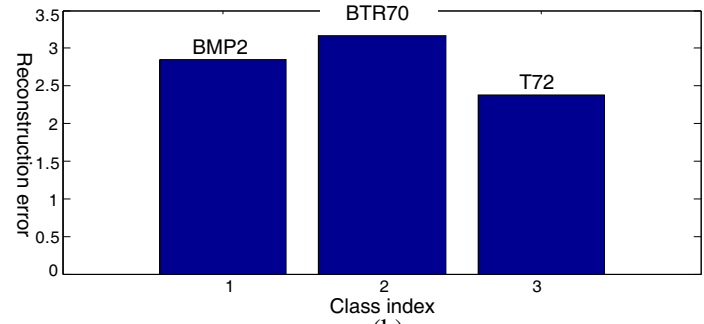

(b)

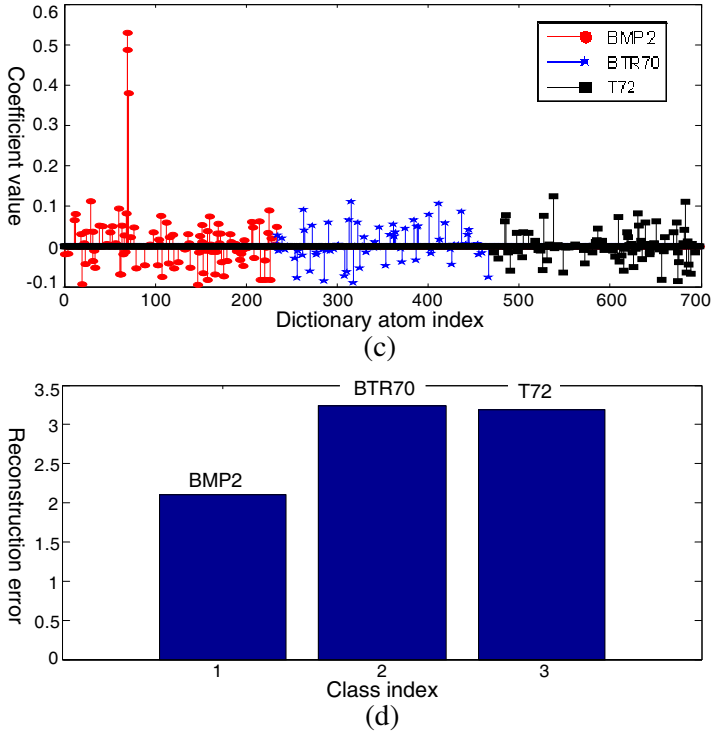

Figure 6. Examples of sparse coefficients and reconstruction errors using BCS classifier with different features: (a) and (b) SAR target image's amplitude values, (c) and (d) scattering centers features.

image amplitude values. The results in Tables 2–3 reveal that BCS achieves an average accuracy of 97.9% with scattering centers features, 89.5% with image amplitude values. From Tables 2–3, it can be seen that the classification performance of BCS is superior to other classifier with the same features. This is because BCS is able to adaptively select representative basis for each test sample compared to other methods. It is also observed that scattering centers features outperform SAR image amplitude values with all classifiers owing to removal of clutter and artifacts. All results confirm the validity and high performance of the proposed approach for SAR ATR.

The base line for the comparison is the template matching method [36]. For our approach, it can be seen that the misclassification error is 2.1% from Table 2. However, it is noted that the proposed method in this paper does not require target pose estimation unlike template method.

Table 3. Classification accuracy comparison of different classifiers with SAR target image amplitude values.

Features		SAR image amplitude values			
Classifier		BP	SRC	SVM	BCS
Target	BMP2	80.9%	71.8%	62.7%	83.3%
	BTR70	83.4%	80.2%	75.3%	95.6%
	T72	79.5%	79.1%	64.9%	89.7%
ARA		81.3%	77.0%	67.6%	89.5%

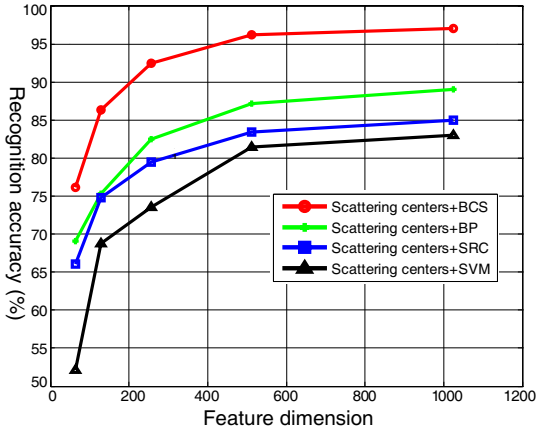

Figure 7. Recognition accuracy with different feature dimensions.

Furthermore, we examine the performance of different classifiers with scattering centers features when feature dimension is changed. The recognition rates is computed with the feature space dimensions 64, 128, 256, 512, and 1024. The corresponding plot is given in Figure 7. As can be seen from Figure 7, the performance of all the feature extraction methods improves as the number of feature dimension increases. However, BCS performs the best among all methods and performs well even in low dimension of 128. It is worthwhile to point out that our approach use only linear computation compared with SVM exploiting nonlinearity by kernel mapping. Overall, the performance of the proposed method is desirable under all feature dimensions evaluated here, indicating the effectiveness of the proposed method.

4.3. Robustness to Noise

In addition, we consider the effect of noise to classification performance of the proposed approach. We add different level Gaussian noise to original data to evaluate the robustness of the method. Figure 8 shows how recognition accuracy varies as the signal-to-noise ratio (SNR) varies from 0 dB to 35 dB. From Figure 8, one can identify that BCS with scattering centers features achieves more than 90% accuracy in the high SNR range between 20–35 dB, and it decreases rapidly at the SNR levels below 10 dB. But, from the results in Figure 8, it can be seen that BCS with scattering centers features is superior to the other methods for the whole SNR range.

4.4. Depression

Because the test target SAR images may be obtained from different depression angle, the adaption of a classification algorithm to

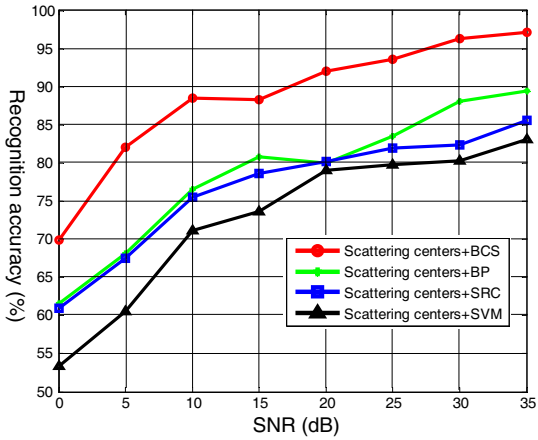

Figure 8. Average recognition accuracy of different methods with different SNR.

Table 4. Depression angle invariance results using different methods with scattering centers features.

Depression angle of testing dataset	methods			
	BP	SRC	SVM	BCS
15°	92.7%	94.3%	89.5%	99.2%
30°	81.9%	82.4%	70.2%	89.6%
45°	65.3%	68.9%	59.1%	70.8%

depression angle is important for real application. The invariance to depression angle for all methods is examined. The dataset in this experiment are summarized in Table 4, which is a subset of the MSTAR database on 3 different targets (BRDM2, ZSU23/4 and 2S1) at four different depression angles (15°, 17°, 30°, 45°). The data at depression angle 17° are used for training and the data at other depression angles for testing. The experiment results are summarized in Table 4. As can be seen from Table 4, all methods have good classification performance when there is a small change of 2° from 17° to 15° in the depression angle. The proposed approach performs more robustly when depression angle change is large, such as a change of 13° from 17° to 30°. However, when the change in the depression angle is very large, such as a change of 28° from 17° to 45°, the performances of all methods obviously decrease because of target signatures dramatic change.

4.5. 10-class Problem

In this subsection, the performance of the proposed method is evaluated on the more challenging 10-class problem, i.e., discriminating between all the 10 classes in the MSTAR database (see Table 1). In this experiment, we use the images from serial number SN_C21 for BMP2 and SN_132 for T72 respectively. We carry out experiments with the

Table 5. Classification results of 10-class problem using different methods.

Target	method			
	BP	SRC	SVM	BCS
BMP2	81.0%	80.0%	65.5%	85.6%
BTR60	86.7%	81.0%	67.7%	93.3%
BTR70	84.7%	79.6%	62.2%	90.3%
BRDM2	75.2%	75.2%	72.8%	92.3%
D7	78.5%	73.7%	70.9%	96.7%
T62	76.2%	70.0%	61.4%	89.7%
T72	70.9%	66.3%	60.5%	95.3%
ZIL131	81.0%	77.4%	72.5%	93.1%
ZSU234	79.2%	78.1%	70.2%	95.3%
2S1	77.0%	78.5%	68.6%	93.8%
ARA	79.0%	76.0%	67.2%	92.6%

same methods using in 3-class problem and the recognition accuracy of each target are summarized in Table 5. From the experiment results, it can be seen that the BCS with scattering centers features achieves an average correct classification rate of 92.6%. We can also find that the proposed method outperform the other feature extraction methods with a large margin, which indicates the superiority of the proposed method.

The obtained recognition accuracy of the proposed method on 10-class SAR ATR tasks is also competitive with previously reported results. In [11], on 10-class SAR ATR tasks they employed hidden markov model (HMM) classifier with HRR profiles features to give the best accuracy of 92.2%. Unlike the method in [11], the proposed method of this paper does not require the complex conversion from SAR image chips to HRR profiles.

5. CONCLUSION

In this paper, we present a new technique of SAR target classification via BCS with scattering centers features. SAR target scattering centers features are extracted as a l_1-norm regularization problem with sparsity constraint based on SAR observation physical model. The extracted scattering centers features can reserve dominant point scattering centers and suppress most artifacts and clutter simultaneously. We show how BCS is applied to construct classifiers for SAR ATR. In experiments, the proposed approach is compared with BP, SRC and SVM using SAR image amplitude values and scattering centers features respectively. Experimental results on the popular MSTAR public release SAR database demonstrate that the proposed approach obtains promising performance on SAR target classification and exhibits strong robustness to noise. It's worth pointing out that the proposed approach can acquire high recognition accuracy without target poses to be known or estimated. Our future work will be done to investigate multiple features based compressive sensing for SAR target classification to improve classification accuracy.

ACKNOWLEDGMENT

This work is supported by the Fundamental Research Funds for the Central Universities of China under Grant No. CDJRC11160003 and No. CDJXS10 16 11 13. This work is also supported by Natural Science Foundation Project of CQ CSTC under Grant No. cstcjjA40018 and No. cstc2012jjB0123.

REFERENCES

1. An, D. X., Z.-M. Zhou, X.-T. Huang, and T. Jin, "A novel imaging approach for high resolution squinted spotlight SAR based on the deramping-based technique and azimuth NLCS principle," *Progress In Electromagnetics Research*, Vol. 123, 485–508, 2012.
2. Chen, J., J. Gao, Y. Zhu, W. Yang, and P. Wang, "A novel image formation algorithm for high-resolution wide-swath spaceborne SAR using compressed sensing on azimuth displacement phase center antenna," *Progress In Electromagnetics Research*, Vol. 125, 527–543, 2012.
3. Tian, B., D.-Y. Zhu, and Z.-D. Zhu, "A novel moving target detection approach for dual-channel SAR system," *Progress In Electromagnetics Research*, Vol. 115, 191–206, 2011.
4. Chiang, C.-Y., Y.-L. Chang, and K.-S. Chen, "SAR image simulation with application to target recognition," *Progress In Electromagnetics Research*, Vol. 119, 35–57, 2011.
5. Dudgeon, D.-E. and R.-T. Lacoss, "An overview of automatic target recognition," *The Lincoln Laboratory Journal*, Vol. 6, 3–9, 1993.
6. Huan, R.-H. and Y. Pan, "Target recognition for multi-aspect SAR images with fusion strategies," *Progress In Electromagnetics Research*, Vol. 134, 267–288, 2013.
7. Papson, S. and R.-M. Narayanan, "Classification via the shadow region in SAR imagery," *IEEE Trans. on Aerospace and Electronic Systems*, Vol. 48, 969–980, 2012.
8. Huang, C.-W. and K.-C. Lee, "Application of ICA technique to PCA based radar target recognition," *Progress In Electromagnetics Research*, Vol. 105, 157–170, 2010.
9. Lee, K.-C., J.-S. Ou, and M.-C. Fang, "Application of SVD noise-reduction technique to PCA based radar target recognition," *Progress In Electromagnetics Research*, Vol. 81, 447–459, 2008.
10. Runkle, P., L.-H. Nguyen, J.-H. McClellan, and L. Carin, "Multi-aspect target detection for SAR imagery using hidden Markov models," *IEEE Trans. on Geoscience and Remote Sensing*, Vol. 39, 46–55, 2001.
11. Liao, X.-J., P. Runkle, and L. Carin, "Identification of ground targets from sequential high-range-resolution radar signatures," *IEEE Trans. on Aerospace and Electronic Systems*, Vol. 38, 1230–1242, 2002.
12. Han, S.-K., H.-T. Kim, S.-H. Park, and K.-T. Kim, "Efficient radar target recognition using a combination of range profile and

time-frequency analysis," *Progress In Electromagnetics Research*, Vol. 108, 131–140, 2010.

13. Potter, L.-C. and R.-L. Moses, "Attributed scattering centers for SAR ATR," *IEEE Trans. on Image Processing*, Vol. 6, 79–91, 1997.
14. Gerry, M.-J., L.-C. Potter, I.-J. Gupta, and A.-V. Merwe, "A parametric model for synthetic aperture radar measurements," *IEEE Trans. on Antennas and Propagation*, Vol. 47, 1179–1188, 1999.
15. Park, S.-H., J.-H. Lee, and K.-T. Kim, "Performance analysis of the scenario-based construction method for real target ISAR recognition," *Progress In Electromagnetics Research*, Vol. 128, 137–151, 2012.
16. Zhao, Q. and J.-C. Principe, "Support vector machines for SAR automatic target recognition," *IEEE Trans. on Aerospace and Electronic Systems*, Vol. 37, 643–654, 2001.
17. Tan, C.-P., J.-Y. Koay, K.-S. Lim, H.-T. Ewe, and H.-T. Chuah, "Classification of multi-temporal SAR images for rice crops using combined entropy decomposition and support vector machine technique," *Progress In Electromagnetics Research*, Vol. 71, 19–39, 2007.
18. Zhang, Y. and L. Wu, "An MR brain images classifier via principal component analysis and kernel support vector machine," *Progress In Electromagnetics Research*, Vol. 130, 369–388, 2012.
19. Angiulli, G., D. De Carlo, G. Amendola, E. Arnieri, and S. Costanzo, "Support vector regression machines to evaluate resonant frequency of elliptic substrate integrate waveguide resonators," *Progress In Electromagnetics Research*, Vol. 83, 107–118, 2008.
20. Wu, Y., Z.-X. Tang, B. Zhang, and Y. Xu, "Permeability measurement of ferromagnetic materials in microwave frequency range using support vector machine regression," *Progress In Electromagnetics Research*, Vol. 70, 247–256, 2007.
21. Candès, E.-J. and M.-B. Wakin, "An introduction to compressive sampling," *IEEE Signal Processing Magazine*, Vol. 25, 21–30, 2008.
22. Candès, E.-J. and T. Tao, "Decoding by linear programming," *IEEE Trans. on Information Theory*, Vol. 51, 4203–4215, 2005.
23. Donoho, D.-L., "Compressed sensing," *IEEE Trans. on Information Theory*, Vol. 52, 1289–1306, 2006.
24. Wei, S.-J., X.-L. Zhang, and J. Shi, "Linear array SAR imaging

via compressed sensing," *Progress In Electromagnetics Research*, Vol. 117, 299–319, 2011.

25. Wright, J., A.-Y. Yang, A. Ganesh, S.-S. Sastry, and Y. Ma, "Robust face recognition via sparse representation," *IEEE Trans. on Pattern Analysis and Machine Intelligence*, Vol. 31, 210–227, 2009.
26. Zhang, S., X. Zhao, and B. Lei, "Robust facial expression recognition via compressive sensing," *Sensors,* Vol. 12, 3747–3761, 2012.
27. Zhang, H., N.-M. Nasrabadi, Y. Zhang, and T.-S. Huang, "Multi-view automatic target recognition using joint sparse representation," *IEEE Trans. on Aerospace and Electronic Systems*, Vol. 48, 2481–2497, 2012.
28. Ji, S., Y. Xue, and L. Carin, "Bayesian compressive sensing," *IEEE Trans. on Signal Processing*, Vol. 56, 2346–2356, 2008.
29. Potter, L.-C., E. Ertin, J.-T. Parker, and M. Çetin, "Sparsity and compressed sensing in radar imaging," *Proceedings of the IEEE*, Vol. 98, 1006–1020, 2010.
30. Zhou, J., Z. Shi, X. Cheng, and Q. Fu, "Automatic target recognition of SAR images based on global scattering center model," *IEEE Trans. on Geoscience and Remote Sensing*, Vol. 49, No. 10, 3713–3729, 2011.
31. Çetin, M. and W.-C. Karl, "Feature-enhanced synthetic aperture radar image formation based on nonquadratic regularization," *IEEE Trans. on Image Processing,* Vol. 10, 623–631, 2001.
32. Chen, S.-S., D.-L. Donoho, and M.-A. Saunders, "Atomic decomposition by basis pursuit," *SIAM Review*, 129–159, 2001.
33. Tibshirani, R., "Regression shrinkage and selection via the lasso," *Journal of the Royal Statistical Society. Series B (Methodological)*, Vol. 58, 267–288, 1996.
34. Tipping, M.-E., "Sparse Bayesian learning and the relevance vector machine," *Journal of Machine Learning Research*, Vol. 1, 211–244, 2001.
35. Xu, J., Y. Pi, and Z. Cao, "Bayesian compressive sensing in synthetic aperture radar imaging," *IET Radar, Sonar & Navigation*, Vol. 6, 2–8, 2012.
36. Zhao, Q., J.-C. Principe, V.-L. Brennan, D. Xu, and Z. Wang, "Synthetic aperture radar automatic target recognition with three strategies of learning and representation," *Optical Engineering*, Vol. 39, 1230–1244, 2000.